RESEARCH ARTICLE

Open Access

Carnosic Acid improves the growth performance of Rice Field Eel (*Monopterus albus*) fed a high-carbohydrate diet: regulation of hepatic glycolipid metabolism, attenuation of liver injury, and restoration of intestinal health

2026 Volume 3, Article number: e022

https://doi.org/10.48130/animadv-0026-0007

Received: 7 January 2026

Revised: 12 February 2026

Accepted: 23 March 2026

Published online: 6 August 2026

Yingming Xie[1], Jinchang Yang[2], Xu Yang[2], Meizhi Zhang[3], Kai Xie[3], Quan Li[3], Yi Hu[3*] and Shude Xu[3*]

[1] Dongguan Mingnong Biotechnology Co., Ltd., Dongguan 523000, China
[2] Guangzhou Yuebao Biotechnology Co., Ltd., Guangzhou 510000, China
[3] Fisheries College, Hunan Agricultural University, Changsha 410128, China
* Correspondence: huyi740322@163.com (Hu Y); xushude0106@hunau.edu.cn (Xu S)

Abstract

Metabolic disorders frequently occur in fish reared under aquaculture models where dietary protein is substituted with high levels of carbohydrates. This study aimed to evaluate the efficacy of carnosic acid (CA) in alleviating the metabolic disorders induced by a high-carbohydrate (HC) diet, focusing on growth performance, hepatic health, and gut microbiota. Four isonitrogenous diets were formulated: A control group (CON; 43% crude protein, 6% crude lipid), an HC group (supplemented with 20% corn starch), and two treatment groups receiving the HC diet supplemented with 0.05% (CA1) and 0.2% (CA2) CA. Following an 8-week feeding trial, the results indicated that CA effectively mitigated the growth retardation and hepatic injury caused by the HC diet. The underlying mechanisms included (1) improving intestinal morphological integrity and significantly enhancing digestive enzyme activities (lipase, amylase, trypsin), thereby promoting nutrient digestion and absorption; (2) upregulating the activities and gene expression of glycolytic enzymes (glucokinase [GK], pyruvate kinase [PK], and phosphofructokinase [PFK]) and downregulating gluconeogenic enzymes (phosphoenolpyruvate carboxykinase [PEPCK], glucose-6-phosphatase [G6Pase], and fructose-1-5-bisphosphatase [Fbpase]), while simultaneously suppressing lipogenesis-related genes (*srebp1*, *acc*, *fas*) and promoting fatty acid beta-oxidation genes (*pparα*, *aco*, *cpt1*), thus reducing abnormal hepatic glycolipid accumulation; (3) lowering hepatic reactive oxygen species levels, boosting antioxidant enzyme activities (catalase [CAT], sodium dismutase [SOD], glutathione peroxidase [GPX]), and inhibiting the expression of inflammation-related genes (*nfkb*, *tlr3*, *il-1β*), thereby alleviating liver damage; and (4) increasing gut microbial diversity and suppressing the abundance of potential pathogens (*g_unclassified_Enterobacteriaceae* and *g_Acinetobacter*). In conclusion, 0.2% CA alleviates the negative metabolic impacts of HC diets on fish through multipathway mechanisms, providing a potential strategy for the sustainable development of aquaculture.

Keywords: *Monopterus albus*, Carnosic acid, High-carbohydrate diet, Glycolipid metabolism, Gut microbiota

Citation: Xie Y, Yang J, Yang X, Zhang M, Xie K, et al. 2026. Carnosic Acid improves the growth performance of Rice Field Eel (*Monopterus albus*) fed a high-carbohydrate diet: regulation of hepatic glycolipid metabolism, attenuation of liver injury, and restoration of intestinal health. *Animal Advances* 3: e022 https://doi.org/10.48130/animadv-0026-0007

Introduction

The sustainable expansion of aquaculture is currently hampered by the volatile supply of fishmeal, a situation exacerbated by the overexploitation of marine stocks. Simultaneously, conventional high-protein formulations often lead to excessive ammonia nitrogen discharge, which conflicts with ecological farming mandates. Consequently, substituting dietary protein with cost-effective carbohydrates has become a pivotal strategy for economic and "green" transitions. However, research indicates that many fish species, particularly carnivores, possess a constrained capacity for carbohydrate utilization, attributed to suboptimal glucose metabolism and endocrine regulation[1,2]. These physiological limitations cause surplus glucose to be redirected toward hepatic glycogen and lipid synthesis. Chronic accumulation often imposes a severe metabolic load, potentially precipitating insulin resistance and systemic metabolic dysfunction[3]. In channel catfish (*Ictalurus punctatus*), for instance, long-term high-carbohydrate (HC) intake has been shown to disrupt glycolipid homeostasis and suppress growth[4]. Moreover, HC diets in grass carp (*Ctenopharyngodon idella*) can alter microbial profiles and compromise the intestinal barrier's integrity, elevating disease risks[5]. Thus, developing interventions to mitigate these HC-induced adverse effects is a critical priority for sustainable industry development.

Carnosic acid (CA), a prominent lipophilic diterpenoid phenol, is widely distributed within Lamiaceae plants, including rosemary, perilla, and sage. It is characterized primarily by its robust antioxidant and anti-inflammatory activities. Mechanistically, CA mitigates oxidative stress by transitioning from a catechol to a quinone form, which subsequently binds to cysteine residues on Keap1. This interaction triggers the liberation and nuclear translocation of *nrf2*, thereby bolstering cellular antioxidant defenses[6]. Regarding its anti-inflammatory profile, CA significantly inhibits the secretion of pro-inflammatory mediators such as *tnf-α* and *il-1β*[7]. Furthermore, CA exerts substantial influence on metabolic regulation. Studies in mice and mammalian cells have demonstrated that CA activates the sirt1/foxo1

https://doi.org/10.48130/animadv-0026-0007

pathway, thereby downregulating adipogenic factors such as *ppary* and *fas*, while upregulating the lipolytic enzyme atgl, ultimately alleviating lipid accumulation[8]. In terms of glucose homeostasis, studies in mice have also shown that CA promotes glucose uptake and sensitizes insulin signaling via the *ampk* pathway[9]. Additionally, CA modulates the intestinal microbial composition, counteracting dysbiosis linked to metabolic resistance[10]. Recent studies in aquaculture have also begun to explore the potential of CA. For instance, dietary CA has been shown to enhance antioxidant capacity and flesh quality in large-mouth bass (*Micropterus salmoides*)[7]. Although these protective mechanisms have been thoroughly characterized in mammals, the regulatory role of CA in the glycolipid metabolism and intestinal health of aquatic species remains poorly understood.

The rice field eel (*Monopterus albus*) is a commercially significant carnivorous fish in China's aquaculture sector. However, the industry's reliance on high-protein dietary formulations has led to escalating production costs. Our previous studies demonstrated that chronic HC intake disrupts hepatic glycolipid homeostasis, induces liver damage, and causes intestinal microbial dysbiosis in this species[11]. Though incorporating carbohydrates is economically advantageous, effective nutritional interventions to mitigate these metabolic health risks are still lacking. Building on the established antioxidant and metabolic-regulating properties of CA observed in mammals, this research systematically evaluates the potential of CA to counteract the growth suppression and metabolic impairments induced by HC diets in *M. albus*. Specifically, we focus on the mechanisms through which CA alleviates hepatic injury and restores gut health, providing a theoretical foundation for its application in sustainable aquafeeds.

Materials and methods

Diet preparation

In this study, a control diet (CON) was designed to provide 43% crude protein and 6% crude lipid, fulfilling the nutritional standards for *M. albus*[12]. The protein matrix consisted of fish meal and wheat gluten, whereas fish oil and corn starch were utilized as the lipid and carbohydrate sources. Based on the CON diet, a high-carbohydrate (HC) diet was developed by increasing the corn starch content by 20%. The CA-supplemented groups (CA1 and CA2) were derived from the HC diet through the inclusion of 0.05% and 0.2% CA, respectively (Table 1). The dosage of CA (0.05% and 0.2%) was selected on the basis of previous studies in our laboratory, where these levels showed efficacy without toxicity.

The preparation process involved grinding all raw materials into a fine powder and weighing them accurately. To ensure uniform distribution, CA was first premixed with a small amount of starch and then progressively mixed with the remaining dry ingredients. Subsequently, all ingredients were blended in a V-shaped mixer for 15 min. Following the mixing stage, the diets were air-dried and stored under cool, desiccated conditions to preserve their nutritional integrity.

Experimental rearing and management

In total, 480 healthy *M. albus* (average weight: 28.00 ± 0.01 g) were sourced from a commercial facility in Changde, Hunan, China. The individuals were randomly distributed into 12 nylon net cages (2.0 m × 1.5 m × 1.5 m), each stocking 40 fish. The study utilized a randomized design with four dietary groups (CON, HC, CA1, and CA2), each conducted in triplicate. Before the trial, the eels underwent a 7-day acclimation period during which they were fed the basal diet. Following a 24-h fast, the 8-week feeding experiment was initiated.

Feeding was performed once per day (17:00–18:30) until apparent satiation was reached, typically requiring a ration of 3%–5% of total biomass. Uneaten feed was collected 1 h after feeding, dried at 65 °C, and weighed to correct the total feed intake. Water parameters were strictly regulated to ensure a stable environment: The temperature was kept at 28.6 ± 1.8 °C; dissolved oxygen, pH, and ammonia nitrogen were maintained at 6.5 ± 0.4, 7.2 ± 0.3, and 0.23 ± 0.03 mg/L, respectively.

Table 1. Composition and nutrient level of the experimental diets (%, dry matter).

Ingredient	CON	HC	CA1	CA2
Fish meal	40	40	40	40
Wheat gluten	14.46	14.46	14.46	14.46
Corn starch	20	40	40	40
Microcrystalline cellulose	20.5	0.5	0.45	0.3
Fish oil	2	2	2	2
Choline	0.5	0.5	0.5	0.5
Premix[1]	1	1	1	1
$Ca(H_2PO_4)_2$	1.5	1.5	1.5	1.5
Antioxidants[2]	0.01	0.01	0.01	0.01
Mold inhibitor[3]	0.03	0.03	0.03	0.03
Carnosic acid (CA)[4]	0	0	0.05	0.2
Nutrition levels[4]				
Crude protein	43.52	43.77	43.89	43.81
Crude lipid	5.92	5.88	5.86	5.91
Ash	9.92	9.73	9.85	9.86

1, Provided by MGO Ter Bio-Tech Co., Ltd. (Qingdao, China). Composition of the vitamin and mineral premix (mg/kg diet): KI (1%), 100 mg; $CoCl_2{\cdot}6H_2O$ (1%), 50 mg; $CuSO_4{\cdot}5H_2O$, 4 mg; $FeSO_4{\cdot}H_2O$, 120 mg; $ZnSO_4{\cdot}H_2O$, 60 mg; $MnSO_4{\cdot}H_2O$, 150 mg; $Na_2SeO_3{\cdot}5H_2O$ (1%), 10 mg; $MgSO_4{\cdot}H_2O$, 30 mg; Vitamin B1, 5 mg; riboflavin, 8 mg; Vitamin B6, 6 mg; Vitamin B12, 0.02 mg; Vitamin K3, 5 mg; inositol, 100 mg; pantothenic acid, 20 mg; niacin acid, 30 mg; folic acid, 1.7 mg; biotin, 0.05 mg; Vitamin A, 15 mg; Vitamin D3, 0.375 mg; Vitamin E, 40 mg; Vitamin C, 100 mg. 2, The main component of the antioxidants is ethoxyquin. 3, The main component of the mold inhibitor is calcium propionate. 4, Purchased from Hunan Zhiyi Biotechnology Co., Ltd (purity ≥ 95%).

Sampling procedures

At the conclusion of the 8-week feeding trial, three fish per replicate were randomly harvested and anesthetized. Fecal specimens were aseptically collected and stored at −80 °C for subsequent 16S rRNA gene sequencing of the gut microbiome. Following a 24-h starvation period, the remaining eels were counted and weighed to determine their growth performance. Subsequently, eight individuals per cage were randomly selected for tissue sampling. Blood was drawn from the caudal vein of four fish and permitted to clot overnight at 4 °C. Serum was then isolated via centrifugation (3,000 rpm, 10 min) and preserved at −80 °C for biochemical assays. From the remaining four fish, the liver and intestinal tissues were excised and weighed to calculate the hepatosomatic index (HSI). Subsamples of these tissues were fixed in 4% paraformaldehyde for histological evaluation, and the remnants were snap-frozen in liquid nitrogen and stored at −80 °C for the biochemical and molecular analyses. Additionally, whole livers from two extra fish per cage were collected and stored at −80 °C specifically for analyzing hepatic glycogen and crude lipid levels.

Histomorphological examination

To evaluate the tissue architecture, the paraformaldehyde-fixed hepatic and intestinal segments (n = 1 per cage) were dehydrated, cleared, and paraffin-embedded according to routine histopathological protocols. Microtome sections were then prepared from these blocks and subjected to hematoxylin and eosin (H&E) staining. Visualization and image acquisition were performed with a Nikon Eclipse Ci-L microscope. Furthermore, a Jiangfeng KF-FL-020 automated digital scanning system was utilized to digitize the stained sections, ensuring comprehensive

observation of the tissue morphology. For morphometric analysis, five randomly selected intact villi per section were measured for villus height (VH) and muscular thickness (MT) at 15× magnification. Goblet cells (GCs) were enumerated in five random fields per slide. All measurements were conducted in a blinded manner to minimize bias.

Serum biochemical profiling

To evaluate systemic metabolism and liver health, freeze–thawed serum samples (n = 2 per cage) were assayed for several key parameters, including glucose (GLU, A154-2-1) and triglycerides (TG, A110-1-1). Hepatic enzymatic activities, specifically glutamic-pyruvic transaminase (GPT, C009-2-1) and glutamic-oxaloacetic transaminase (GOT, C010-2-1), were also quantified. These analyses were performed following the standardized procedures provided by the kit manufacturer (Nanjing Jiancheng Bioengineering Institute, Nanjing, China) using colorimetric methods.

Determination of tissue biochemical parameters

Liver and intestinal samples (n = 2 per cage) from each replicate were homogenized in ice-cold physiological saline (1:9 w/v ratio) utilizing a mechanical homogenizer. Following centrifugation, the supernatants were harvested for further enzymatic quantification.

The following physiological parameters were determined.

Intestinal digestive capacity: Activities of amylase (AMS, A054-2-1), lipase (LPS, A054-2-1), and trypsin (TRY, JL-T1273).

Hepatic glucose metabolism: Key glycolytic enzymes including glucokinase (GK, JL-T1046), phosphofructokinase (PFK, JL-T0976), and pyruvate kinase (PK, JL-T0767) and gluconeogenic enzymes including glucose-6-phosphatase (G6Pase, JL-T1038), fructose-1, 6-bisphosphatase (FBPase, JL-T0888), and phosphoenolpyruvate carboxykinase (PEPCK, JL-T0635).

Oxidative status: Indicators including reactive oxygen species (ROS, JL-T3037), malondialdehyde (MDA, A006-2-1), and the antioxidant defense system, specifically catalase (CAT, A007-1-1), superoxide dismutase (SOD, A001-3-2), glutathione peroxidase (GPx, A005-1-2), and glutathione (GSH, A006-2-1).

Diagnostic kits for glucose metabolism enzymes and ROS were procured from Jianglai Biotechnology Co., Ltd., whereas all other parameters were analyzed using kits from Nanjing Jiancheng Bioengineering Institute. All procedures strictly followed the manufacturers' standardized protocols.

Analysis of hepatic transcript levels

For molecular analysis, Trizol-based extraction was used to obtain total RNA from hepatic tissues (n = 2 per cage). The high quality of the isolated RNA was substantiated by A_{260}/A_{280} ratios of 1.8–2.0 and the presence of intact bands revealed by agarose gel electrophoresis. After the synthesis of cDNA, relative gene expression was analyzed by quantitative polymerase chain reaction (qPCR). All primer (Table 2) pairs demonstrated specific amplification, characterized by unique melting peaks and efficiencies ranging from 90% to 110%. Target gene normalization was performed against the reference gene *rpl17* using the $2^{-\Delta\Delta C_T}$ method. The specific compositions of the reaction mixtures and the qPCR thermocycling conditions are documented in Supplementary File 1.

Gut microbiota profiling via *16S* rRNA sequencing

Microbial genomic DNA was isolated from representative fecal specimens (n = 1 per cage) utilizing a commercial extraction kit. The quality and concentration of the extracted DNA were validated via spectrophotometric (A_{260}/A_{280}) analysis and agarose gel electrophoresis. To characterize the bacterial communities, the V3–V4 hypervariable regions of the *16S* rRNA gene were targeted for PCR amplification. The resulting libraries were sequenced on an Illumina MiSeq platform (USA) using a 300-bp paired-end strategy. Raw sequence data were processed within the QIIME 2 framework (v2020.6). After primer removal, the DADA2 pipeline was used for quality filtration, denoising, and sequence merging, ultimately generating a feature table of amplicon sequence variants (ASVs). Following taxonomic assignment, low-abundance ASVs (relative frequency < 0.1% across any sample) were excluded to ensure the robustness of the subsequent statistical analyses.

Table 2. Real-time PCR primer sequences.

Gene	Forward primer (5'-3')	Reverse primer (5'-3')	Accession No.
rpl17	CGAGAACCCGACTAAATCA	GTTGTAGCGACGGAAAGG	XM_020587712.1
gk	AAGCCATCGTATCCCACC	GGGTCCCAGTCCATAGTGT	XM_020620531.1
pk	CCGCCAAGGGACTGTTT	CCACTGGTGGTAAGGACTATG	XM_020617665.1
pfk	AGCATAGGAGCAGACACCG	CACAGAATCCACCCATAGTC	XM_020594803.1
pepck	CTGTGACGGCTCTGACG	ATACATGGTGCGACCTTTC	XM_020621224.1
fbpase	GGTATGAGGGTCTGTTTAGC	GACAGCCACCCAGATGA	XM_020616553.1
g6pase	GCTGCGGTTGCTGTATG	TTCTTGGCGTGTTTATGG	XM_020585913.1
srebp1	ATCAGCGGTAAGCCAGTCGG	CAGCCACCAGGTCTTTGAGC	XM_020616413.1
acc	TCTGACAGCGACCCCTTCT	GCCCCACACATTCTTATTGC	XM_020598745.1
fas	CTGTCCGAGGCGGCATAAT	CCTGTTCCTTCCCCTTCTGG	XM_020608884.1
pparα	TGACAGAGTTCGCTAAGGCAGTG	CATCTTTGTTCATGCAGGAGGC	XM_020621872.1
aco	CTTTGGCTCTGTTCTACACCTTG	CATGGATGTCAAAGGCATCTACC	XM_020610963.1
cpt1	CCTGGAAGAAGCGTGTCATCAGAC	TGACTGGCAGGTGCTCCTGTATC	XM_020625222.1
nrf2	CTTCAGACAGCGGTGACAGG	GCCTCATTCAGTTGGTGCTT	XM_020596409.1
sod	AGCTGGCTAAGTTCTCATTCAC	GCAGTAACATTGCCCAAGTCT	XM_020598413.1
cat	GTCCAAGTCTAAGGCATCTCC	CTCCTCTTCGTTCAGCACC	XM_020624985.1
gpx1	GTTCACCGCCAAACTCTT	TTCCCATTCACATCTACCTT	XM_020607739.1
gstk	TTGATGTTCCCCTGCGTTAT	CACCTGCTCTACCTGCTTGTC	XM_020610780.1
nfκb	ACCCTACCGTGACACTAACCT	TGCCGTCTATCTTGTGGAAT	XM_020616319.1
tlr3	TATTTAGAGCCATACAGGG	CACAATCAAGAACGCACA	XM_020614353.1
il1β	GAGATGTGGAGCCCAAACTT	CTGCCTCTGACCTTCTGGACTT	KM113037.1

rpl17: ribosomal protein L17; *gk: glucokinase*; *pk: pyruvate kinase*; *pfk: phosphofructokinase*; *pepck: phosphoenolpyruvate carboxykinase*; *fbpase: fructose-1,6-bisphosphatase*; *g6pase: glucose-6-phosphatase*; *srebp1: sterol regulatory element-binding protein 1*; *acc: acetyl-CoA carboxylase*; *fas: fatty acid synthase*; *pparα: peroxisome proliferator-activated receptor alpha*; *aco: acyl-CoA oxidase*; *cpt1: carnitine palmitoyltransferase 1*; *nrf2: nuclear factor erythroid 2-related factor 2*; *sod: superoxide dismutase*; *cat: catalase*; *gpx1: glutathione peroxidase 1*; *gstk: glutathione S-transferase kappa*; *nfκb: nuclear factor kappa B subunit*; *tlr3: toll-like receptor 3*; *il1β: interleukin-1 beta*.

https://doi.org/10.48130/animadv-0026-0007

Data processing and computational methods

All quantitative data were processed with SPSS, with scientific illustrations produced using Python to ensure high-quality visualization. Prior to the comparative analysis, the underlying assumptions of parametric tests—normality and homoscedasticity—were rigorously assessed via the Shapiro–Wilk and Bartlett procedures. When both criteria were met, differences between groups were identified via one-way analysis of variance (ANOVA) followed by Tukey's post-hoc analysis. Conversely, non-normal or heteroscedastic datasets were analyzed using the Kruskal–Wallis *H*-test. Post-hoc comparisons for nonparametric data were conducted using Dunn's test. For the microbiome analysis, the linear discriminant analysis effect size (LEfSe) was used to identify differentially abundant taxa, with an LDA score threshold of > 2.0 and $p < 0.05$. The results were considered to be statistically significant at $p < 0.05$.

Results

Growth performance and intestinal digestion and absorption

The survival rate (SR) of *M. albus* remained statistically similar across all treatments throughout the trial ($p > 0.05$, Fig. 1d). Significant differences were recorded in growth performance, where the HC group exhibited lower weight gain rate (WGR) and higher feed coefficient (FCR) values relative to the CON group ($p < 0.05$, Fig. 1b, c). For intestinal structural indices, VH, MT, and GC counts were significantly reduced in eels fed the HC diet compared with those in the CON group ($p < 0.05$, Fig. 1e–h). Similarly, the HC group displayed significantly lower intestinal lipase (LPS) and trypsin (TRY) activities, alongside significantly higher amylase (AMS) activity ($p < 0.05$, Fig. 1i–k). Dietary CA inclusion altered these parameters: The CA2 group showed significantly higher WGR, VH, MT, and GC counts and LPS/TRY activities, together with a significantly lower FCR, in comparison with the HC group ($p < 0.05$).

Hepatic glycolipid metabolism

Long-term consumption of the HC diet significantly increased hepatosomatic index (HSI), hepatic crude lipid (HCL), and hepatic glycogen content (HGC) levels compared with the CON group ($p < 0.05$, Fig. 2a–c). Serum levels of TG and GLU were also significantly higher in the HC group ($p < 0.05$, Fig. 2d, e). In the CA-supplemented groups, HSI, HCL, HGC, and serum TG and GLU were significantly lower than those recorded in the HC group ($p < 0.05$).

Regarding glucose metabolism, the HC group exhibited significantly higher activities of glycolytic enzymes (GK, PK, PFK) and upregulated mRNA expression of their corresponding genes (*gk*, *pk*, *pfk*) compared with the CON group ($p < 0.05$, Fig. 2f–h, l–n). Conversely, the activities and gene expression levels of gluconeogenic enzymes (PEPCK, G6Pase, and Fbpase) were significantly lower in the HC group than in the CON group ($p < 0.05$, Fig. 2i–k, o–q). Dietary CA supplementation resulted in significantly higher glycolytic enzyme activities and gene expression levels compared with the HC group ($p < 0.05$), whereas the activities and transcript levels of gluconeogenic enzymes were significantly lower ($p < 0.05$).

In terms of lipid metabolism, the HC group showed significantly higher expression of lipogenic genes (*srebp1*, *acc*, *fas*) and significantly lower expression of fatty acid beta-oxidation genes (*pparα*, *aco*, *cpt1*) compared with the CON group ($p < 0.05$, Fig. 2r–w). In the CA-supplemented groups, the expression of *srebp1*, *acc*, and *fas* was significantly lower, whereas the expression of *pparα*, *aco*, and *cpt1* was significantly higher than in the HC group ($p < 0.05$).

Liver tissue injury

As shown in Fig. 3a, b, the HC group exhibited higher levels of hepatocellular vacuolation and a significantly lower number of nuclei compared with the CON group ($p < 0.05$). These morphological observations were coupled with significantly higher serum GOT and GPT activities in HC-fed eels ($p < 0.05$, Fig. 3c, d). Following CA administration, an increase in nucleus number and a decrease in serum GOT and GPT were recorded relative to the HC group ($p < 0.05$).

In terms of oxidative status, the HC group displayed significantly lower activities of CAT, SOD, and GPX, as well as lower GSH concentrations ($p < 0.05$, Fig. 3g–j). Similarly, the transcript levels of *nrf2*, *sod*, *cat*, *gpx1*, and *gstk* were significantly reduced in the HC group ($p < 0.05$, Fig. 3k–o). Conversely, hepatic ROS and MDA levels were significantly higher in the HC group, accompanied by significantly higher expression of *nfkb*, *tlr3*, and *il1β* ($p < 0.05$, Fig. 3e, f, p–r). Dietary inclusion of CA resulted in significantly higher antioxidant enzyme activities and gene expression levels, alongside significantly lower ROS and MDA levels and proinflammatory gene expression compared with the HC group ($p < 0.05$).

Characteristics of the gut microbial community structure

Phylogenetic analysis based on ASVs identified p_Proteobacteria and *g_Clavibacter* as the most prevalent phylum and genus across all groups, respectively (Fig. 4a). The total ASV counts for the CON, HC, CA1, and CA2 groups were 52, 24, 56, and 85, respectively. Among these, the number of unique ASVs was 15 (CON), 18 (HC), 20 (CA1), and 44 (CA2), with only 1 ASV shared by all four groups (Fig. 4b). Alpha diversity analysis showed that the Shannon and Simpson indices were significantly lower in the HC group than in the CON group ($p < 0.05$, Fig. 4c, d). In contrast, these indices were significantly higher in the CA-supplemented groups compared with the HC group ($p < 0.05$). Principal coordinate analysis (PCoA) using Bray–Curtis distances (two-dimensional and three-dimensional) revealed distinct clustering and separation of the microbial communities among the treatments (Fig. 4e, f).

At the phylum level (Fig. 4g), p_Proteobacteria, p_Actinobacteria, and p_Firmicutes were the dominant taxa. The relative abundance of p_Proteobacteria was higher, whereas that of p_Actinobacteria was lower in the HC group than in the CON group. Relative to the HC group, the CA-supplemented groups showed a lower abundance of p_Proteobacteria and a higher abundance of p_Actinobacteria. At the genus level (Fig. 4h), the dominant genera in the CON, CA1, and CA2 groups included *g_Rhizobiales*, *g_Clavibacter*, *g_Actinomycetales*, and *g_Methylosinus*. In the HC group, *g_unclassified_Enterobacteriaceae* and *g_Acinetobacter* were the predominant genera, accounting for a combined relative abundance of 97.99%.

Identification of core microbes

According to the LDA scores from the LEfSe analysis, p_Proteobacteria, p_Actinobacteria, p_Chloroflexi, p_Planctomycetes, and p_Bacteroidetes were identified as the most differentially abundant phyla among groups (Fig. 5a). The top five genera showing significant discrimination included *g_unclassified_Enterobacteriaceae*, *g_Rhizobiales*, *g_Acinetobacter*, *g_Clavibacter*, and *g_Methylosinus* (Fig. 5b). At the ASV level, several features (e.g., ASV_19730, ASV_2693, ASV_39414, and ASV_33037) were significantly more abundant in the HC group ($p < 0.05$, Fig. 5c) and were taxonomically linked to *_Acinetobacter* and *g_unclassified_Enterobacteriaceae*. The results of the Mantel test showed that the relative abundances of these HC-enriched ASVs significantly correlated with growth metrics, liver biochemical parameters, and hepatic inflammatory indices ($p < 0.05$, Fig. 5d).

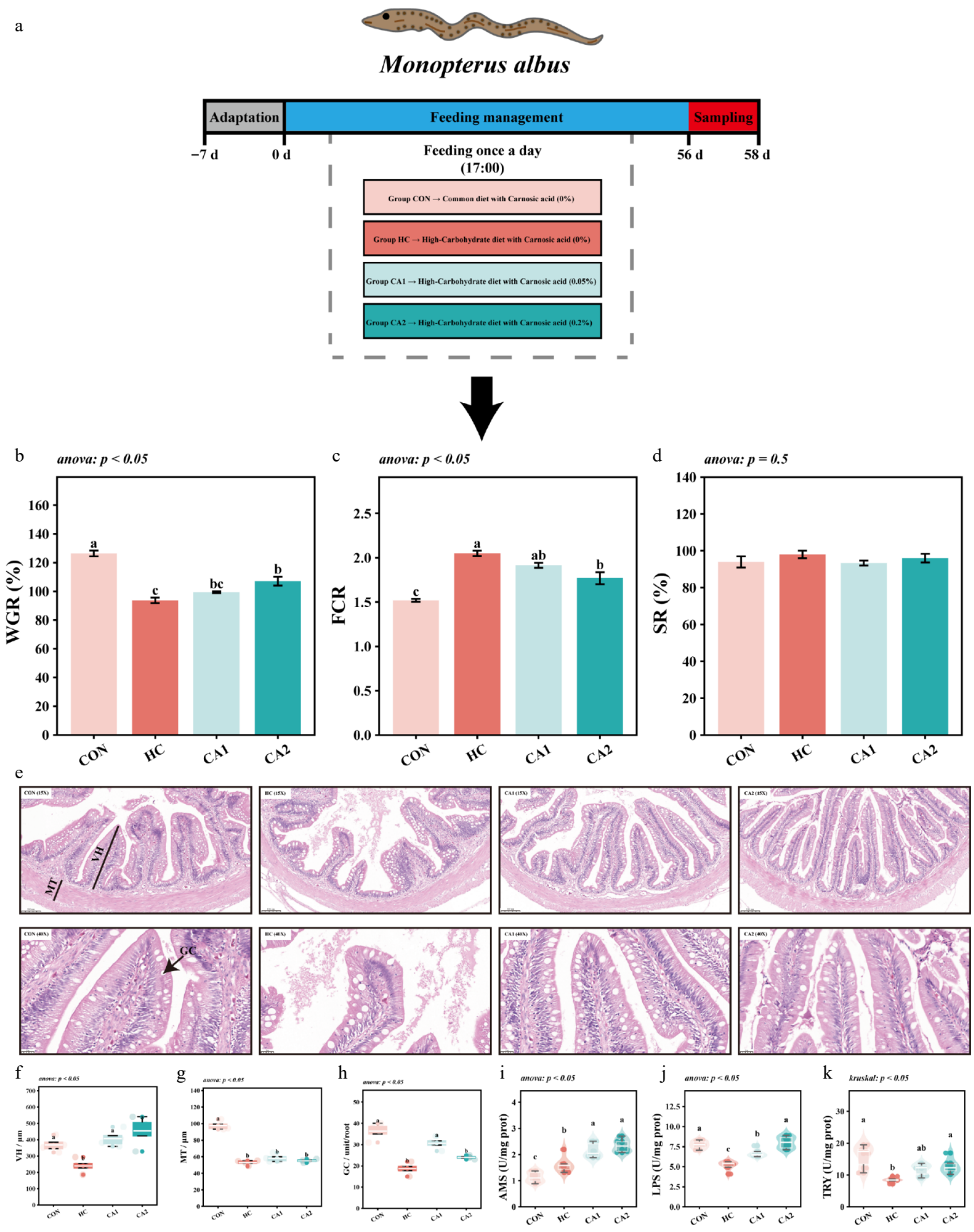

Fig. 1 Growth performance and intestinal digestion and absorption. (a) Feeding strategy of *M. albus* during the experimental period; (b) WGR (%): Weight gain rate = 100 × (Final body weight − Initial body weight) / Initial body weight; (c) FCR: Feed coefficient = Feed weight / (Final body weight − Initial body weight); (d) SR (%): Survival rate = 100 × Final number / Initial number. (e) H&E staining of the intestine. (f) Villus height (VH), μm. (g) Muscular thickness (MT), μm. (h) Goblet cells (GCs) per unit/root. (i) Amylase (AMS), units (U)/mg protein. (j) Lipase (LPS), U/mg protein. (k) Trypsin (TRY), U/mg protein.

https://doi.org/10.48130/animadv-0026-0007

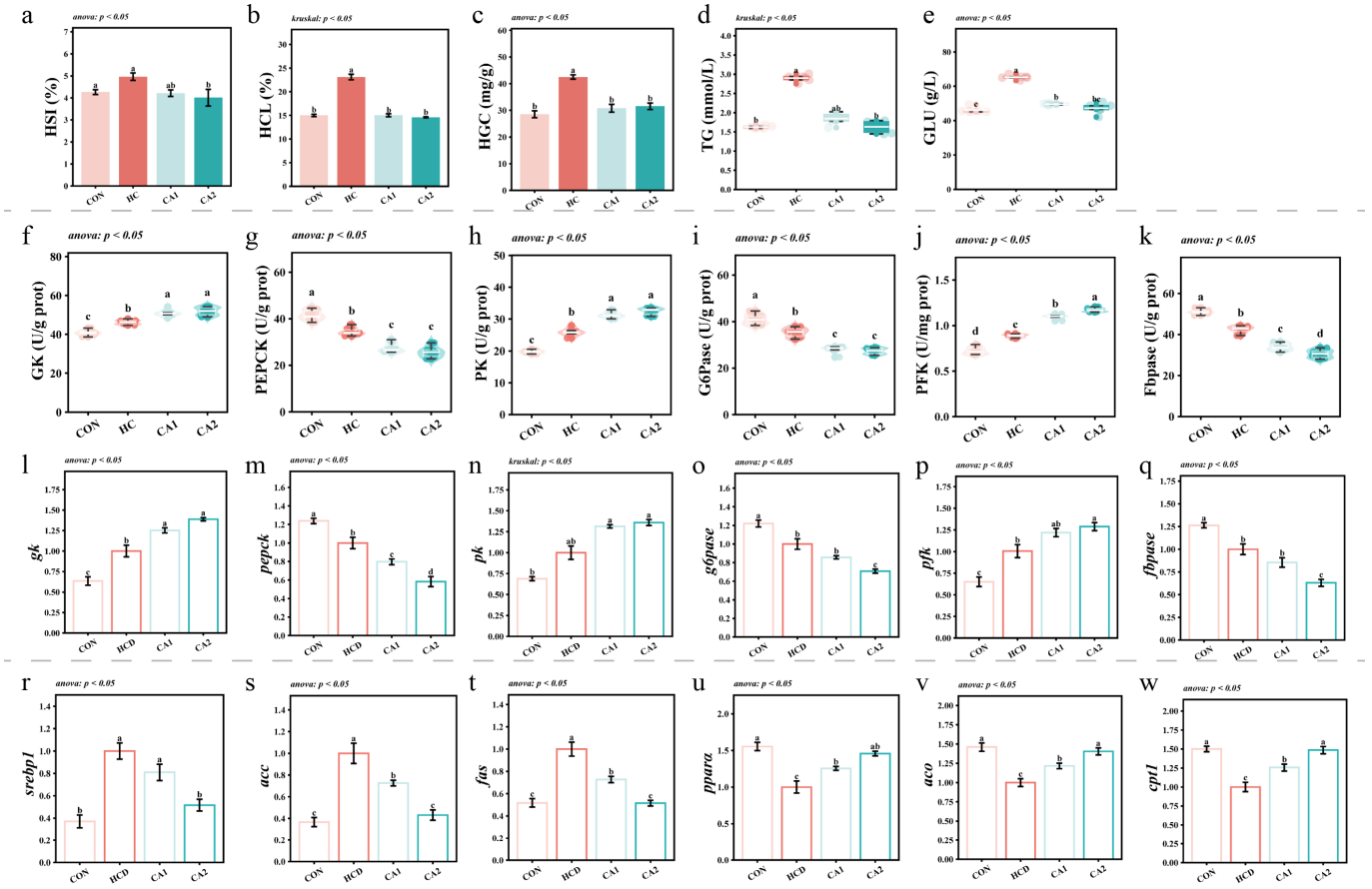

Fig. 2 Hepatic glycolipid metabolism. (a) Hepatosomatic index (HSI, in %) = 100 × Liver weight / Body weight. (b) HCL, %; (c) HGC, mg/g; (d) serum TG, mmol/L; (e) serum GLU, g/L; (f) GK, U/g protein; (g) PEPCK, U/g protein; (h) PK, U/g protein; (i) G6pase, U/g protein; (j) PFK, U/mg protein; (k) Fbpase, U/g protein. (l) *gk*: *glucokinase*; (m) *pepck*: *phosphoenolpyruvate carboxykinase*; (n) *pk*: *pyruvate kinase*; (o) *g6pase*: *glucose-6-phosphatase*; (p) *pfk*: *phosphofructokinase*; (q) *fbpase*: *fructose-1,6-bisphosphatase*; (r) *srebp1*: *sterol regulatory element-binding protein 1c*; (s) *acc*: *acetyl-coa carboxylase*; (t) *fas*: *fatty acid synthase*; (u) *pparα*: *peroxisome proliferator-activated receptor alpha*; (v) *aco*: *acyl-coA oxidase*; (w) *cpt1*: *carnitine palmitoyltransferase 1*.

Discussion

Carnosic acid enhances growth performance by improving intestinal structure and function

Economic viability in aquaculture relies heavily on growth performance. Our data reveal that adding CA to the diet mitigates the growth suppression caused by feeding on HC rations. This beneficial outcome appears to stem from CA-mediated enhancements in both intestinal integrity and digestive function. It is widely established that fish exhibit poor glucose tolerance[13]. Extended exposure to carbohydrate-rich diets typically disrupts intestinal function and impedes growth[14], a trend corroborated by our findings. Here, CA treatment effectively counteracted the detrimental impacts of excess carbohydrates on the gut. Morphologically, CA improved intestinal structure, supporting physical digestion. Functionally, it rebalanced the enzyme profiles by boosting TRY and LPS activities, which were inhibited by the HC diet. This suggests that CA not only protects the structural barrier but also restores the enzymatic capacity required for efficient nutrient assimilation. By optimizing the digestive enzyme spectrum, CA likely improves the utilization of nutrients, thereby ensuring adequate nutrient substrates to fuel growth.

Carnosic acid alleviates the metabolic burden by remodeling hepatic glucose and lipid homeostasis

The conversion of absorbed nutrients into somatic growth relies on their efficient metabolism within the liver. Conversely, prolonged exposure to HC diets frequently results in the excessive deposition of glycogen and lipids in hepatic tissue. This trend, previously observed across various fish species[15,16], was corroborated by our data. Significantly, the inclusion of CA in the diet successfully attenuated the hepatic accumulation of glucose and lipids triggered by HC intake. Fundamentally, the retention of hepatic lipids and glycogen represents a morphological consequence of disrupted metabolic homeostasis, stemming from a lack of coordination between the synthesis and degradation pathways[17,18]. Our findings indicate that CA upregulated key enzymes involved in glycolysis, thereby facilitating glucose breakdown while suppressing gluconeogenesis to limit glycogen buildup. Furthermore, when carbohydrate intake surpasses immediate energy requirements and glycogen storage limits, the surplus is diverted toward triglyceride synthesis via *de novo* lipogenesis, causing fatty liver[19,20]. We observed that CA treatment mitigated this by repressing fatty acid synthesis and enhancing β-oxidation, ultimately lowering the hepatic fat content. Collectively, CA modulated metabolic pathways, specifically by boosting glycolysis and fatty acid oxidation while restraining gluconeogenesis and lipogenesis. This systemic regulation optimized hepatic carbohydrate utilization and minimized lipid formation, effectively counteracting the metabolic disturbances and hepatic deposition associated with HC diets.

Carnosic acid protects hepatocytes by attenuating oxidative stress and inflammatory responses

The accumulation of excess lipids in the liver is a primary pathological driver of hepatic injury[21,22]. Our data demonstrate that adding CA to the

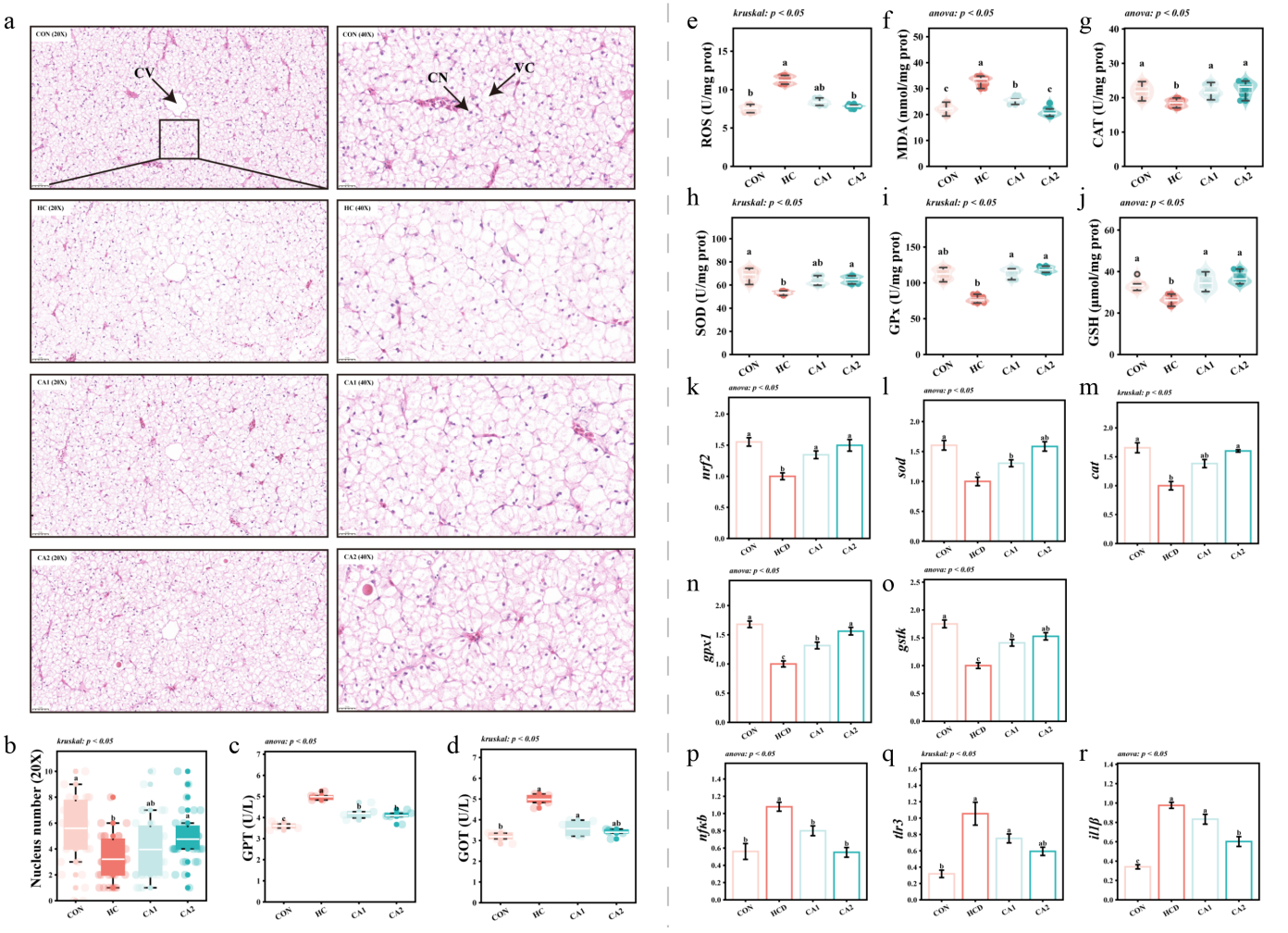

Fig. 3 Liver tissue injury. (a) Results of H&E staining of the liver: CV, central veins (the veins in the center of the hepatic lobule are surrounded by radial liver cells, which are important vessels for the exchange of substances between the liver and other organs); CN, cell nucleus; VC, vacuolization cell. (b) The number of hepatic cell nuclei; (c) GPT, U/L; (d) GOT, U/L; (e) ROS, U/mg protein; (f) MDA, nmol/mg protein; (g) CAT, U/mg protein; (h) SOD, U/mg protein; (i) GPX, U/mg protein; (j) GSH, μmol/mg protein. (k) *nrf2*: *nuclear factor erythroid 2-related factor*; (l) *sod*: *superoxide dismutase*; (m) *cat*: *catalase*; (n) *gpx1*: *glutathione peroxidase 1*; (o) *gtsk*: *glutathione S-transferase kappa*; (p) *nfkb*: *nuclear factor kappa b*; (q) *tlr3*: *toll-like receptor 3*; (r) *il1β*: *interleukin-1 beta*.

diet successfully attenuated hepatic damage caused by HC intake. This protection appears to be mediated through the mitigation of lipid-induced oxidative stress and inflammation. Lipids stored in excess are susceptible to oxidation, a process that intensifies metabolic pressure and leads to a surge in ROS production, ultimately causing oxidative stress and cell death[23,24]. Concurrently, lipid overload triggers hepatic immune responses, launching inflammatory processes that worsen tissue deterioration[25]. Here, we observed that CA treatment markedly downregulated hepatic ROS levels, boosted antioxidant defenses, and suppressed key inflammatory signaling pathways and the associated cytokines. Collectively, the hepatoprotection provided by CA operates via two distinct mechanisms. First, by modulating metabolic pathways, it limits lipid deposition, thereby relieving metabolic burden at its origin. Second, CA possesses inherent bioactivity that allows it to directly scavenge free radicals and block the cascades of oxidative damage and inflammation.

Carnosic acid ameliorates systemic health via gut microbiota-mediated modulation of inflammation

The gut microbiota is integral to the intestinal microenvironment and is essential for modulating the host's metabolism and systemic balance[26]. A reduction in alpha diversity typically signals compromised intestinal health[27]. Our data show that chronic consumption of an HC diet significantly diminished gut microbial alpha diversity, mirroring patterns observed in other aquatic species[28]. However, the inclusion of CA in the diet successfully counteracted this decline, fostering the restoration of microbial diversity. Taxonomic profiling highlighted a significant surge in the relative abundances of *g_unclassified_Enterobacteriaceae* and *g_Acinetobacter* under HC conditions. It has been documented that *g_unclassified_Enterobacteriaceae* is associated with systemic inflammation; its cell wall derivative, lipopolysaccharide (LPS), is a potent endotoxin. Translocation of LPS into the bloodstream activates cascades such as TLR4/NFKB, driving cytokine storms associated with metabolic endotoxemia and intestinal inflammation[29,30]. Similarly, *g_Acinetobacter*, an opportunistic pathogen, may provoke host inflammation via factors like outer membrane protein A[31]. Statistical correlations linked these specific genera to poor growth, liver damage, and hepatic inflammation. We postulate that HC diets compromise the gut barrier, causing dysbiosis that may exacerbate hepatic injury via the gut–liver axis. Crucially, CA treatment inhibited the expansion of these pathogenic genera and optimized the community structure. This microbial modulation appears to be a primary mechanism by which CA mitigates hepatic inflammation and aids growth recovery. In summary,

https://doi.org/10.48130/animadv-0026-0007

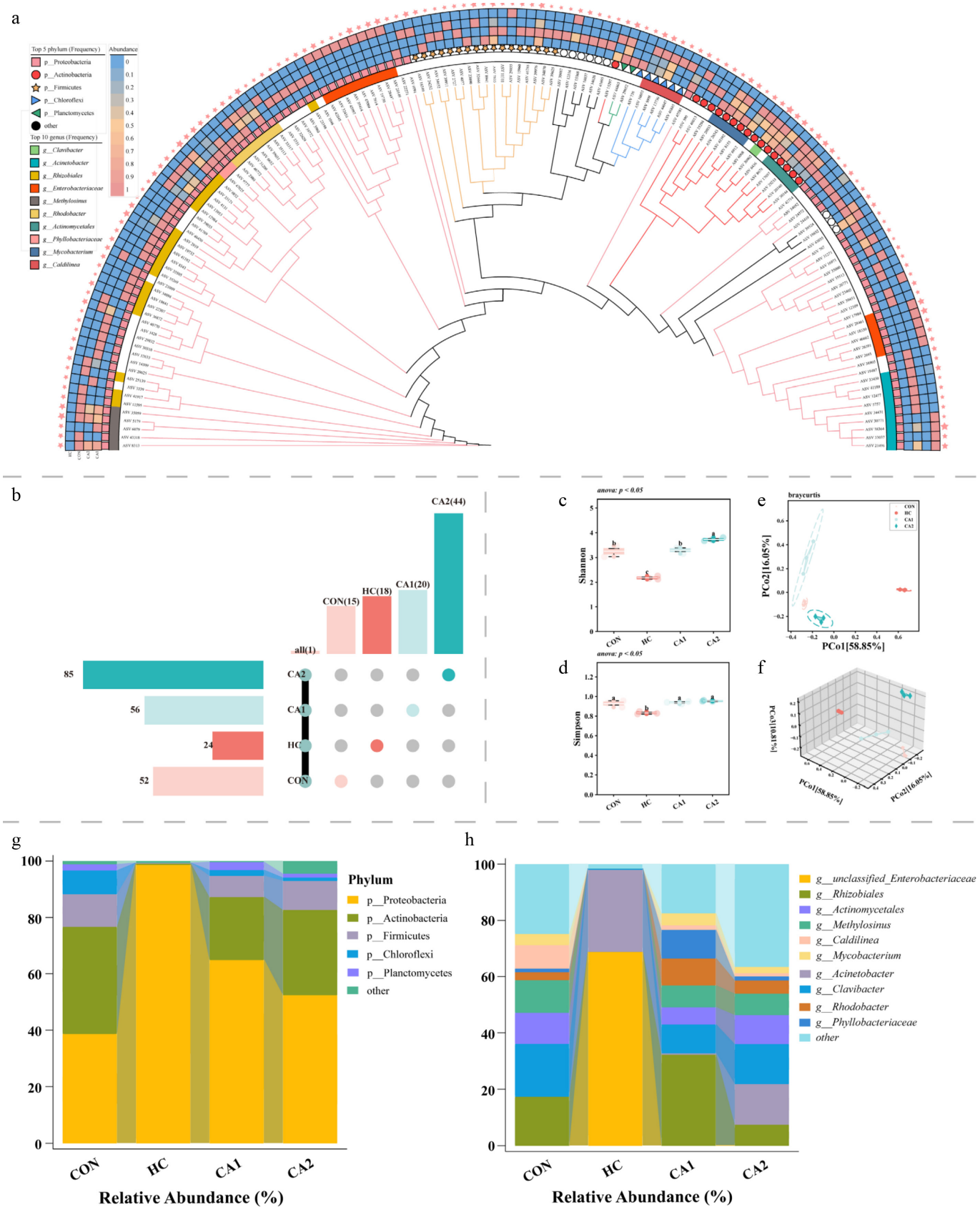

Fig. 4 Characteristics of the gut microbial community structure. (a) Phylogenetic tree constructed based on ASV feature sequences. (b) The upset plot shows the number of ASVs in each group. (c), (d) The Shannon and Simpson indices of alpha diversity. (e), (f) Principal coordinate analysis (PCoA), with two-dimensional (2D) and three-dimensional (3D) plots of samples based on Bray–Curtis distance. (g) The phylum composition of the gut microbiota in each group (top 5). (h) The genus composition of the gut microbiota in each group (top 10).

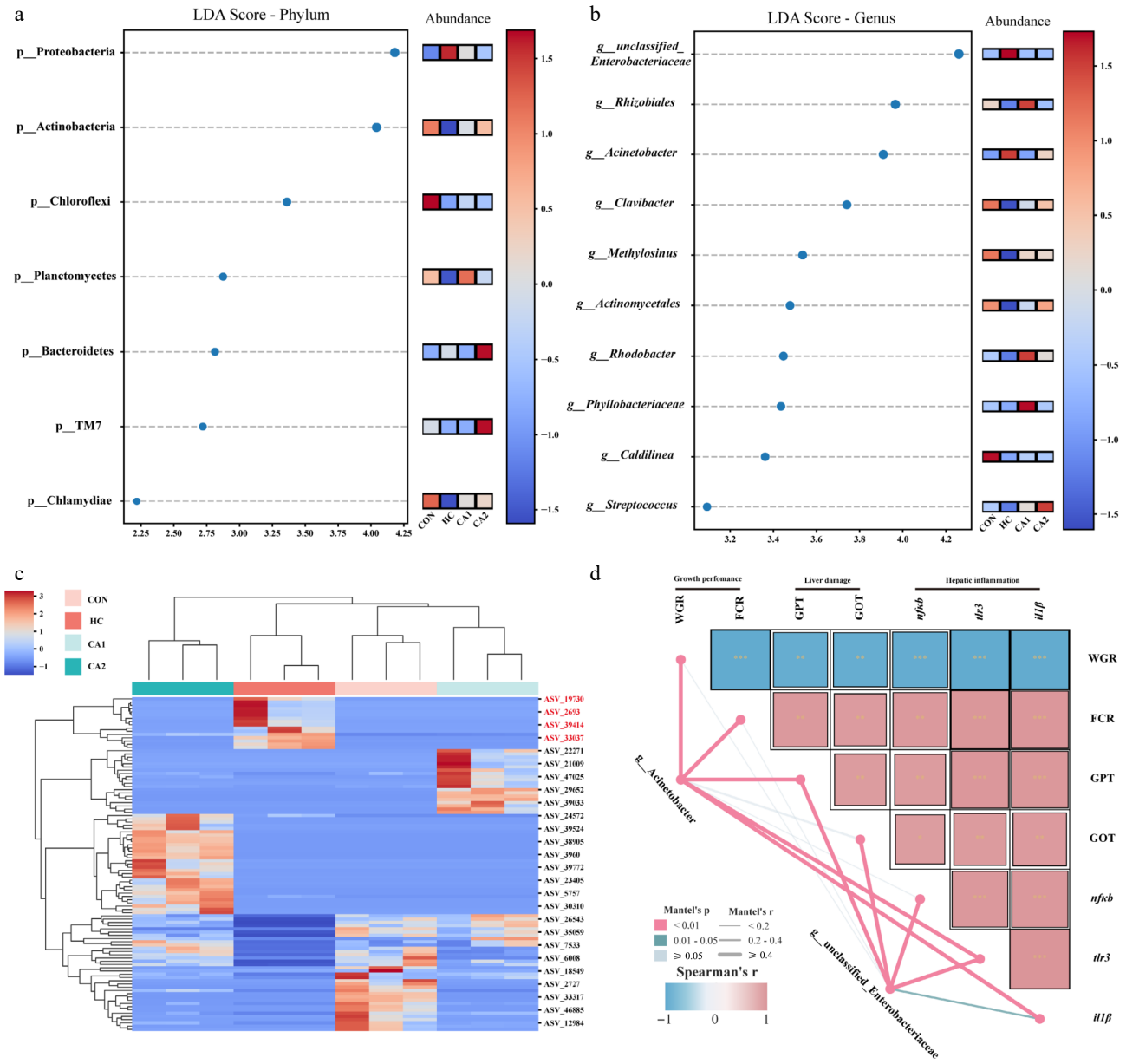

Fig. 5 Identification of core microbes. (a) LEfSe analysis at the phylum level (top 10). (b) LEfSe analysis at the genus level (top 10). (c) LEfSe analysis at the ASV level. (d) Mantel test for specific ASVs (from g_unclassified_Enterobacteriaceae and g_Acinetobacter) and phenotypic indicators.

CA likely provides systemic protection against metabolic inflammation by preserving the gut's integrity and regulating the microbiome through the gut microbiota–liver axis.

Conclusions

Collectively, our data indicate that dietary inclusion of 0.2% CA is the optimal strategy for mitigating the metabolic dysfunction caused by HC diets in *M. albus*. The benefits of CA are realized through several integrated pathways. First, CA improves nutrient utilization by protecting the intestinal morphology and rebalancing digestive enzymes. Second, it regulates hepatic metabolism by promoting the catabolism of glucose and lipids while limiting their synthesis, thus preventing excessive deposition. Third, CA alleviates liver injury by neutralizing oxidative stress and blocking inflammatory cascades. Finally, CA reshapes the intestinal microbiome by reducing pathogenic genera and increasing diversity, which supports liver health through the gut–liver axis. Consequently, CA represents a promising, sustainable feed additive for counteracting the negative effects of carbohydrate-rich diets in aquaculture operations.

Ethical statements

This study was approved by the Committee of Laboratory Animal Management and Animal Welfare of Hunan Agricultural University (Changsha, China), and all experimental procedures conformed to the guidelines of the Ethical Committee of Hunan Agricultural University (approval number: 2025121, approval date: 2025-04-08).

Author contributions

The authors confirm their contributions to the paper as follows: conceptualization, methodology, and writing – original draft preparation: Xie Y, Yang J; software and visualization: Yang X, Zhang M; investigation: Xie K, Li Q; funding acquisition: Hu Y; writing – review and editing: Xu S. All

authors reviewed the results and approved the final version of the manuscript.

Data availability

The datasets generated during and/or analyzed in the current study are available from the corresponding author upon reasonable request.

Acknowledgments

This research was financed by the National Natural Science Foundation of China (32172986). We thank the staff at the Fisheries College for their technical assistance.

Conflict of interest

The authors declare that they have no conflict of interest.

Supplementary information accompanies this paper online at: https://doi.org/10.48130/animadv-0026-0007.

References

[1] Zhao L, Liao L, Tang X, Liang J, Liu Q, et al. 2022. High-carbohydrate diet altered conversion of metabolites, and deteriorated health in juvenile largemouth bass. *Aquaculture* 549:737816

[2] Ji S, Song L, Tian Z, Wei M, Ji H, et al. 2025. Caffeic acid phenethyl ester improves high-carbohydrate diet utilization by promoting adipocyte hyperplasia in grass carp (*Ctenopharyngodon* idellus). *Animal Nutrition* 22:154–164

[3] Polakof S, Panserat S, Soengas JL, Moon TW. 2012. Glucose metabolism in fish: a review. *Journal of Comparative Physiology B* 182:1015–1045

[4] Liu Y, Lu Q, Han G, Zheng Y, Cao J, et al. 2024. Dietary betulinic acid alleviates high carbohydrate diet-induced hepatic *de novo* lipogenesis through AMPK signaling and improves liver health in channel catfish (*Ictalurus punctatus*). *Aquaculture Reports* 36:102187

[5] Zhang Y, Liu Y, Ma H, Sun M, Wang X, et al. 2023. Insufficient or excessive dietary carbohydrates affect gut health through change in gut microbiota and regulation of gene expression of gut epithelial cells in grass carp (*Ctenopharyngodon idella*). *Fish & Shellfish Immunology* 132:108442

[6] Zhang S, Wang Q, Dong J, Li G, Niu K, et al. 2025. Dietary Carnosic Acid supplementation improves the growth performance, the antioxidant status, and diversity of intestinal microbiota in broilers. *Antioxidants* 14:1026

[7] Xu Z, Chen Y, Geng H, Ni H, Han D, et al. 2024. Carnosic acid-riched rosemary (*Rosmarinus officinalis* L.) extract improves largemouth bass (*Micropterus salmoides*)'s disease-resistance and regulates lipid metabolism. *Aquaculture Reports* 37:102262

[8] Liao CH, Hung HC, Lai CN, Liao YH, Liu PT, et al. 2023. Carnosic acid and rosemary extract reversed the lipid accumulation induced by bisphenol A in the 3T3-L1 preadipocytes and C57BL/6J mice *via* SIRT1/FoxO1 pathway. *Food and Chemical Toxicology* 179:113996

[9] Tsakiridis N, Niazur Rahman SM, Tsiani E, Giacca A. 2024. 1521-P: carnosic acid protects against diet-induced insulin resistance. *Diabetes* 73:1521-P

[10] Ou J, Huang J, Zhao D, Du B, Wang M. 2018. Protective effect of rosmarinic acid and carnosic acid against streptozotocin-induced oxidation, glycation, inflammation and microbiota imbalance in diabetic rats. *Food & Function* 9:851–860

[11] Shi Y, Zhong L, Fan Y, Zhang J, Zhong H, et al. 2022. The protective effect of mulberry leaf flavonoids on high-carbohydrate-induced liver oxidative stress, inflammatory response and intestinal microbiota disturbance in *Monopterus* albus. *Antioxidants* 11:976

[12] Ma X, Hu Y, Wang XQ, Ai QH, He ZG, et al. 2014. Effects of practical dietary protein to lipid levels on growth, digestive enzyme activities and body composition of juvenile rice field eel (*Monopterus* albus). *Aquaculture International* 22:749–760

[13] Kamalam BS, Medale F, Panserat S. 2017. Utilisation of dietary carbohydrates in farmed fishes: New insights on influencing factors, biological limitations and future strategies. *Aquaculture* 467:3–27

[14] Zhou YL, He GL, Jin T, Chen YJ, Dai FY, et al. 2021. High dietary starch impairs intestinal health and microbiota of largemouth bass, *Micropterus salmoides*. *Aquaculture* 534:736261

[15] Guo Q, Wang Y, Li N, Li T, Guan Y, et al. 2024. Effects of dietary carbohydrate levels on growth performance, feed utilization, liver histology and intestinal microflora of juvenile tiger puffer, *Takifugu* rubripes. *Aquaculture Reports* 36:102035

[16] Gong Y, Lu Q, Liu Y, Xi L, Zhang Z, et al. 2022. Dietary berberine alleviates high carbohydrate diet-induced intestinal damages and improves lipid metabolism in largemouth bass (*Micropterus salmoides*). *Frontiers in Nutrition Volume* 9:1010859

[17] Samuel VT, Shulman GI. 2018. Nonalcoholic fatty liver disease as a nexus of metabolic and hepatic diseases. *Cell Metabolism* 27:22–41

[18] Petersen MC, Vatner DF, Shulman GI. 2017. Regulation of hepatic glucose metabolism in health and disease. *Nature Reviews Endocrinology* 13:572–587

[19] Lundsgaard AM, Bojsen-Møller KN, Kiens B. 2023. Dietary regulation of hepatic triacylglycerol content—the role of eucaloric carbohydrate restriction with fat or protein replacement. *Advances in Nutrition* 14:1359–1373

[20] Liu X, Wang H, Liang X, Roberts MS. 2017. Hepatic Metabolism in Liver Health and Disease. In *Liver Pathophysiology*, ed. Murie P. Boston, USA: Academic Press. pp. 391–400 doi: 10.1016/B978-0-12-804274-8.00030-8

[21] Geng Y, Faber KN, de Meijer VE, Blokzijl H, Moshage H. 2021. How does hepatic lipid accumulation lead to lipotoxicity in non-alcoholic fatty liver disease? *Hepatology International* 15:21–35

[22] Ipsen DH, Lykkesfeldt J, Tveden-Nyborg P. 2018. Molecular mechanisms of hepatic lipid accumulation in non-alcoholic fatty liver disease. *Cellular and Molecular Life Sciences* 75:3313–3327

[23] Smirne C, Croce E, Di Benedetto D, Cantaluppi V, Comi C, et al. 2022. Oxidative stress in non-alcoholic fatty liver disease. *Livers* 2:30–76

[24] Ezhilarasan D, Lakshmi T. 2022. A molecular insight into the role of antioxidants in nonalcoholic fatty liver diseases. *Oxidative Medicine and Cellular Longevity* 2022:9233650

[25] Sukhorukov VN, Orekhov AN. 2024. Molecular aspects of inflammation and lipid metabolism in health and disease: the role of the mitochondria. *International Journal of Molecular Sciences* 25:6299

[26] Ma WW, Huang ZQ, Liu K, Li DZ, Mo TL, et al. 2024. The role of intestinal microbiota and metabolites in intestinal inflammation. *Microbiological Research* 288:127838

[27] Klimenko ES, Belkova NL, Rychkova LV, Darenskaya MA, Tugarinova OA, et al. 2024. Alpha diversity indices as indicators of the variability of gut microbiota in obese adolescents of different ethnicities. *Bulletin of Experimental Biology and Medicine* 176:591–594

[28] Zhang Y, Liang XF, He S, Chen X, Wang J, et al. 2020. Effects of high carbohydrate diet-modulated microbiota on gut health in Chinese perch. *Frontiers in Microbiology* 11:575102

[29] Zhang C, Teng X, Cao Q, Deng Y, Yang M, et al. 2025. Gut microbiota dysbiosis exacerbates heart failure by the LPS-TLR4/NF-κB signalling axis: mechanistic insights and therapeutic potential of TLR4 inhibition. *Journal of Translational Medicine* 23:762

[30] Baldelli V, Scaldaferri F, Putignani L, Del Chierico F. 2021. The role of Enterobacteriaceae in gut microbiota dysbiosis in inflammatory bowel diseases. *Microorganisms* 9:697

[31] Zhang W, Zhou H, Jiang Y, He J, Yao Y, et al. 2022. *Acinetobacter baumannii* outer membrane protein a induces pulmonary epithelial barrier dysfunction and bacterial translocation through the TLR2/IQGAP1 axis. *Frontiers in Immunology* 13:927955